Global and Planetary Change 184 (2020) 103049

Contents lists available at ScienceDirect

Global and Planetary Change

journal homepage: www.elsevier.com/locate/gloplacha

Research article

Constraining the magnitude of the carbon isotope excursion during the Paleocene-Eocene thermal maximum using larger benthic foraminifera

Qinghai Zhang[a,b,*], Lin Ding[a], Kouki Kitajima[c], John W. Valley[c], Bo Zhang[d], Xiaoxia Xu[a], Helmut Willems[b,e], Andreas Klügel[b]

[a] Key Laboratory of Continental Collision and Plateau Uplift, Institute of Tibetan Plateau Research, Chinese Academy of Sciences, and CAS Center for Excellence in Tibetan Plateau Earth Sciences, Beijing 100101, China
[b] Department of Geosciences, University of Bremen, Bremen 28359, Germany
[c] WiscSIMS, Department of Geoscience, University of Wisconsin, Madison, WI 53706, USA
[d] The Key Laboratory of Orogenic Belts and Crustal Evolution, School of Earth and Space Sciences, Peking University, Beijing 100871, China
[e] Nanjing Institute of Geology and Palaeontology, Chinese Academy of Sciences, Nanjing 210008, China

ARTICLE INFO

Keywords:
Paleocene-Eocene thermal maximum
CIE magnitude
SIMS
Larger benthic foraminifera
Tibet

ABSTRACT

The Paleocene-Eocene thermal maximum (PETM) was an extraordinary pulse of global warming that left an indelible mark on the Earth approximately 56 Ma ago. This warming event is associated with an addition of large amounts of ^{13}C-depleted carbon into the atmosphere-ocean system, but the magnitude of the negative carbon isotope excursion (CIE) signaling the PETM onset and often used to estimate mass of the released carbon is still debated. Here we gauge the CIE magnitude through the use of secondary ion mass spectrometry (SIMS) to perform *in situ* δ^{13}C measurements within individual larger benthic foraminifera preserved in a tropical shallow-marine limestone section at Tingri, south Tibet. This SIMS-based δ^{13}C record yields a CIE ($\mathbf{\Delta}$~7‰) comparable in magnitude to that registered by some terrestrial PETM records but larger than the ~4‰ CIE returned by surface-dwelling planktonic foraminifera in deep-sea records. We posit that the CIE magnitude in the surface ocean and atmosphere was ~7‰, and that previous ~4‰ estimates are attenuated by incomplete preservation and/or diagenetic overprinting. Mass balance calculations indicate that the released carbon mass during the CIE would not exceed 28,000 petagrams, given that the carbon was sourced from organic matter, permafrost, thermogenic methane, methane hydrate, or any of their combinations. Our study demonstrates that δ^{13}C records from some shallow-marine carbonate sections can avoid strong diagenetic alteration, preserving primary signals of deep-time carbon perturbations.

1. Introduction

The Paleocene-Eocene thermal maximum (PETM) was a geologically rapid global warming event that happened ~56 Ma ago and lasted ~200 kyr (Kennett and Stott 1991; Röhl et al. 2007). This event was associated with a perturbation to the global carbon cycle as evidenced by a sharp decrease in the carbon isotope compositions (δ^{13}C) of both inorganic and organic carbon in exogenic carbon pools (Bowen et al. 2001, 2015; Diefendorf et al. 2010; Handley et al. 2008; Kennett and Stott 1991; Koch et al. 1992; Magioncalda et al. 2004; Manners et al. 2013; McInerney and Wing 2011; Pagani et al. 2006; Schmitz and Pujalte 2003; Smith et al. 2007; Zachos et al. 2007). It is widely accepted that thousands of petagrams (Pg) of ^{13}C-depleted carbon was added into the atmosphere-ocean system during the PETM (Dickens et al. 1995; Meissner et al. 2014), which either triggered the initial warming or intensified the warming as a positive feedback (Dickens et al. 1995; Thomas et al. 2002; Zachos et al. 2008). The addition of ^{13}C-depleted carbon caused a ~6–8‰ decrease in the δ^{13}C of paleosol carbonate, enamel apatite, higher plant *n*-alkanes on land and bulk carbonate in shallow-marine environments (Bains et al. 2003; Bowen et al. 2001, 2015; Handley et al. 2008; Koch et al. 1992; Pagani et al. 2006; Schmitz and Pujalte 2003; Zhang et al. 2017). In contrast, the δ^{13}C decrease in the open ocean is estimated at ~4–4.6‰ for mixed-layer planktonic foraminifera (Kozdon et al. 2018; Zachos et al. 2007) and ~2–3.5‰ for thermocline-dwelling planktonic foraminifera and small benthic foraminifera (Kennett and Stott 1991; McCarren et al. 2008; Nunes and Norris 2006; Thomas and Shackleton 1996). The term "carbon isotope excursion" (CIE) was coined to describe this δ^{13}C

* Corresponding author at: Key Laboratory of Continental Collision and Plateau Uplift, Institute of Tibetan Plateau Research, Chinese Academy of Sciences, and CAS Center for Excellence in Tibetan Plateau Earth Sciences, Beijing 100101, China.
E-mail address: zhang@itpcas.ac.cn (Q. Zhang).

https://doi.org/10.1016/j.gloplacha.2019.103049
Received 31 January 2019; Received in revised form 5 September 2019; Accepted 27 September 2019

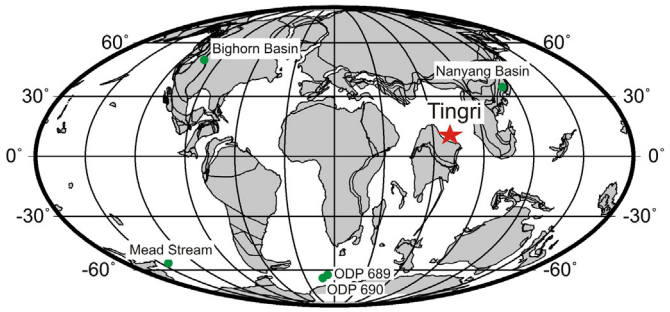

Fig. 1. Plate reconstruction (56 Ma; from ODSN Plate Tectonic Reconstruction Service) showing locations of 13ZS section at Tingri (red star) and other PETM sections preserving the stepped CIE (green dots). (For interpretation of the references to colour in this figure legend, the reader is referred to the web version of this article.)

decrease, and the full CIE magnitude and its remarkable difference from different depositional environments are the subject of much debate (Bowen et al. 2004; Diefendorf et al. 2010; Handley et al. 2008; Kozdon et al. 2018; McInerney and Wing 2011 and references therein; Pagani et al. 2006; Schubert and Jahren 2013; Smith et al. 2007; Tipple et al. 2011; Zachos et al. 2007; Zhang et al. 2017).

It has been argued that the smaller CIE magnitude returned by pelagic sites might result from incomplete preservation stemming from carbonate dissolution fueled by carbon input during the PETM (Pagani et al. 2006; Zachos et al. 2005). The lower part of the CIE stratigraphy in many pelagic PETM sections is marked by clay-rich calcareous ooze associated with an increased fragmentation of planktonic foraminifer shells (Colosimo et al. 2006; Kelly et al. 2012; Zachos et al. 2003) or claystone devoid of sedimentary calcite with a sharp basal contact (Zachos et al. 2005). For instance, the PETM section of Ocean Drilling Program (ODP) Site 690 contains hitherto one of the most complete CIE records recovered from deep-sea sedimentary archives (Fig. 1), yet it has been estimated that as much as ~60% of sedimentary calcite has been lost to dissolution across the PETM onset in this reference section (Bralower et al. 2014). Given that foraminifer weight percentages in bulk sediment are low (~3–9%) (Kelly et al. 2012) and planktonic foraminifera are more susceptible to dissolution than coccoliths (Chiu and Broecker 2008), it is very likely that the foraminiferal record at Site 690 is incomplete. To complicate matters, deep-sea benthic foraminifera experienced a major taxonomic turnover during the PETM with ~30–50 species succumbing to extinction (Thomas and Shackleton 1996). Thus, if one assumes that peak pCO_2 concentrations scale with the severity of carbonate under-saturation and are signaled by the lowest $\delta^{13}C$ value, then it stands to reason that foraminifera recording the most negative $\delta^{13}C$ value of the CIE were dissolved and that deep-sea foraminiferal records might underestimate the true magnitude of the CIE (Pagani et al. 2006).

In some siliciclastic sections formed in shallow-marine environments, the completeness of their PETM records might have also been affected by carbonate dissolution (Bralower et al. 2018). Nevertheless, stratigraphic records of the PETM-CIE from terrestrial sections and many shallow-marine carbonate sections tend to be expanded and are not strongly affected by carbonate dissolution (Andrews et al. 2017; Li et al. 2017; Schmitz and Pujalte 2003; Yans et al. 2006; Zamagni et al. 2012). This does not imply, however, that the complete CIE event is preserved in these records. In these environments, physical erosion or non-deposition frequently occurs and can leave numerous sedimentary hiatuses that may go unrecognized. A voluminous compilation of accumulation rates reveals that net accumulation rates decrease systematically as measurement intervals increase (Fig. 2). This relationship was interpreted as reflecting the incomplete nature of sedimentary records (Sadler 1981, 1999), a phenomenon coined "Sadler effect" (Schumer and Jerolmack 2009). Thus, as measurement intervals increase, longer hiatuses are incorporated into calculation of accumulation rates so that the rates will decrease. As time resolution increases and measurement intervals decrease, some longer hiatuses are revealed, and calculated accumulation rates will increase by avoiding temporal gaps represented by these hiatuses (Sadler 1999). In Sadler's compilation, accumulation rates in terrestrial and shallow-marine environments decrease rapidly as measurement intervals increase from 1 kyr to 100 kyr, which are relevant to the duration of the PETM-CIE (Fig. 2). This suggests that most terrestrial and shallow-marine CIE records are, at least statistically, also incomplete, and that whether the nadir of the $\delta^{13}C$ record is preserved in these sections is largely uncertain. So, the observed large CIE magnitude returned from paleosol carbonate, enamel apatite, higher plant *n*-alkanes from terrestrial sections and bulk carbonate, foraminifera from shallow-marine sections is better to be viewed as a conservative estimate of the CIE magnitude, instead of the full CIE magnitude.

Although it remains challenging to determine the true completeness of PETM-CIE records, some studies suggest that the stepped CIE, consisting of three evident $\delta^{13}C$ decreases (phases **c, e, g**) intervened by slight $\delta^{13}C$ variations (phases **d, f**), likely represents a more complete record of carbon perturbation during the PETM (Bains et al. 1999; Nicolo et al. 2010; Stoll 2005; Zhang et al. 2017; Zhu et al. 2010) (Fig. 3). Several lines of evidence support the fidelity of the stepped CIE records, which are often preserved in bulk carbonate: (1) In pelagic PETM sections, the major component in bulk carbonate is calcareous nannofossils (*i.e.*, coccoliths), and coccoliths have been shown to be more dissolution-resistant than foraminifera on the sea floor (Chiu and Broecker 2008). (2) Some culture experiments suggest that high CO_2 partial pressures can increase the calcification and net primary production in coccolithophores (Iglesias-Rodriguez et al. 2008). Collectively, bulk carbonate records from pelagic PETM sections should suffer less "time loss" than foraminifer records. (3) Inter-species vital effects in coccolith $\delta^{13}C$ during periods of relatively high pCO_2 concentrations ($>$ 375–575 ppm) were believed to be suppressed (Bolton and Stoll 2013; Hermoso et al. 2016). Specifically, Stoll (2005) demonstrated that inter-specific vital effects of coccolith $\delta^{13}C$ during the PETM are very small at ODP Site 690. (4) The stepped CIE at ODP Site 690 was confirmed not to be a consequence of sedimentation rate changes (Farley and Eltgroth 2003). (5) The stepped CIE was also recognized, albeit implicitly, from the $\delta^{13}C$ record of thermocline-dwelling planktonic foraminifer *Subbotina* at ODP Site 690 (see Fig. 4a in Nunes and Norris 2006). (6) The stepped CIE is unlikely caused by bioturbation because it was reported from paleosols at Polecat Bench in the Bighorn Basin (Bains et al. 2003) and from the hemipelagic section at Mead Stream (New Zealand) where no strong bioturbation was observed (Nicolo et al. 2010). (7) The stepped structure of the CIE has been used to correlate PETM sections from geographically distant areas (Bains et al. 1999, 2003; Zhang et al. 2017; Zhu et al. 2010) (Fig. 1). These sections were formed in different depositional environments (open ocean, continental slope, carbonate ramp, lake), presumably representing some of the best preserved PETM sections in these depositional settings (Fig. 3).

Here we constrain the CIE magnitude during the PETM based on a tropical, shallow-marine carbonate section (section 13ZS) at Tingri, south Tibet (Fig. 1). Most of the samples in section 13ZS have $>$ 90–95% carbonate contents (Fig. 4) and are rich in larger benthic foraminifera (LBF). LBF usually dwell in shallow-marine oligotrophic environments, implying insignificant continental river runoff in this area. Thus, section 13ZS has an advantage over sections formed in shallow-marine siliciclastic environments in that the PETM-CIE record in the former is not strongly complicated by river discharge, potentially preserving an "uncontaminated" marine CIE signal. In this study, we conduct *in situ* $\delta^{13}C$ measurements on LBF shells by using secondary ion mass spectrometry (SIMS). To assess possible diagenetic effects on the preservation of LBF shells, we use laser ablation inductively coupled plasma mass spectrometry (LA-ICPMS) to measure *in situ* Sr/Ca, Al/Ca,

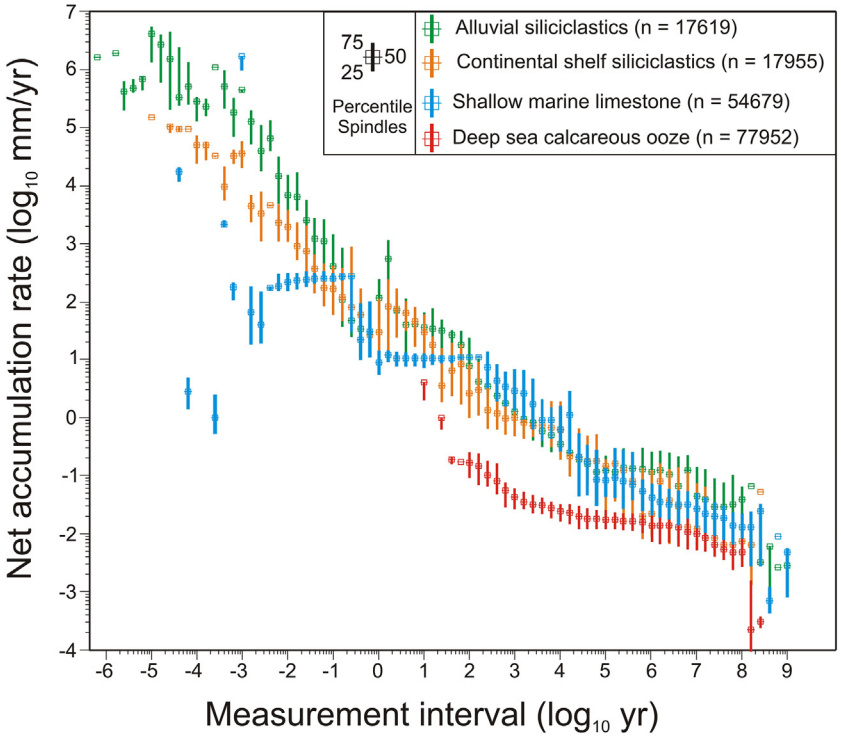

Fig. 2. A compilation of published accumulation rates of sediments in different depositional environments showing power law relationships between net accumulation rates and measurement intervals. Distributions of median, 25th, 75th percentile values are determined for five measurement-interval units per logarithm cycle with no smoothing or overlap (figure courtesy Peter Sadler).

Mn/Ca, Y/Ca, La/Ca, and Ce/Ca ratios from LBF shells. These new data may provide a better constraint on the true CIE magnitude in the surface ocean and improve our understanding of carbon cycling during the PETM.

2. Section, samples and methods

Studied samples are collected from section 13ZS that is exposed at Tingri, south Tibet (Zhang et al. 2017). During the PETM, Tingri was located on a shallow-marine carbonate ramp at ~10° N paleolatitude within the Tethyan Himalaya (van Hinsbergen et al. 2012), and was at least ~300 km away from the southern shoreline of the Neo-Tethyan

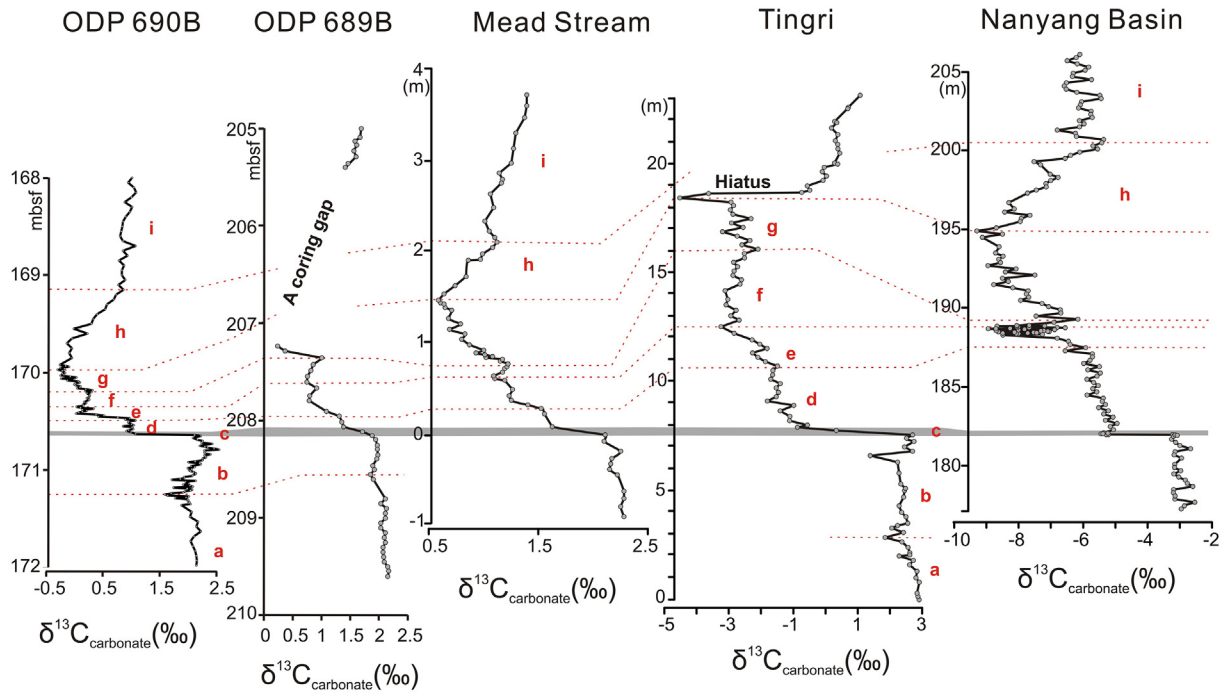

Fig. 3. Correlation of the stepped CIE among pelagic sections (ODP Sites 690B & 689B on Maud Rise, Weddell Sea), a hemipelagic section on the continental slope (Mead Stream, New Zealand), a carbonate section on the shallow-marine carbonate ramp (13ZS section at Tingri, south Tibet), and a lacustrine carbonate section (Yuhuangding section in the Nanyang Basin, China). The grey shading denotes the CIE onset. Raw data are taken from Bains et al. (1999), Kelly et al. (2012), Nicolo et al. (2010), Zhang et al. (2017), and Zhu et al. (2010).

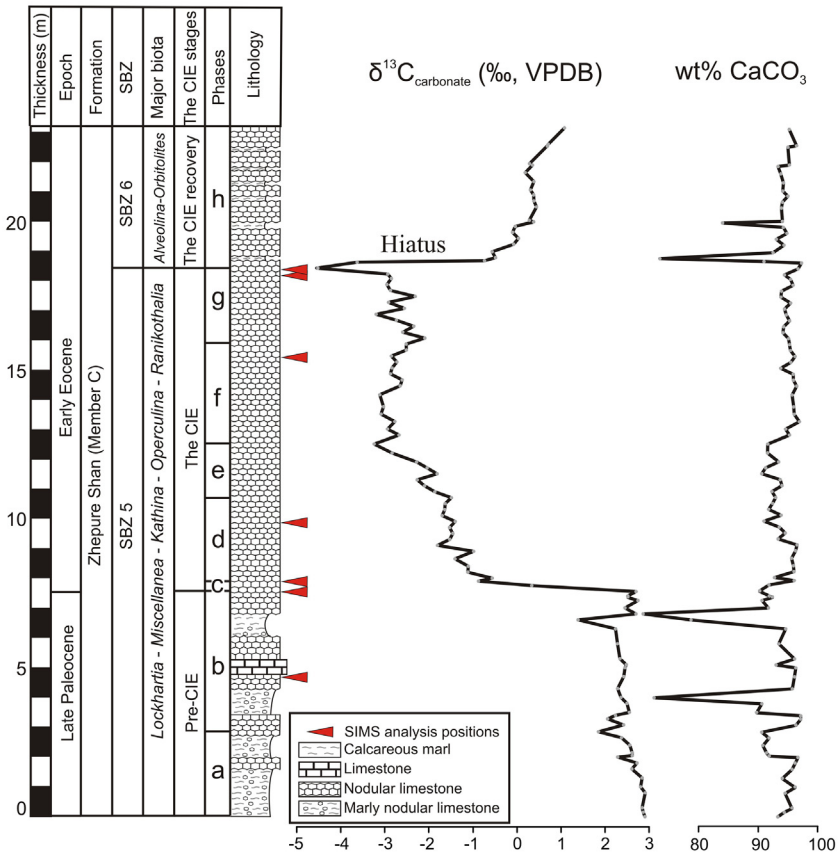

Fig. 4. Lithology, LBF assemblages, Shallow Benthic Zonations (SBZ), CIE stages and phases, bulk carbonate $\delta^{13}C$ and carbonate contents in section 13ZS, revised from Zhang et al. (2017). Red triangles denote stratigraphic positions of SIMS-analyzed samples. The SBZs in section 13ZS were taken from Zhang et al. (2019). (For interpretation of the references to colour in this figure legend, the reader is referred to the web version of this article.)

Ocean (Zhang et al. 2017).

Section 13ZS is ~22 m thick and comprises calcareous marl, marly nodular limestone, and nodular limestone (Fig. 4). The dominant components in limestone samples are micrites and LBF fragments, with minor clay and sparry calcites (Fig. 5A). A sedimentary hiatus and a sudden change in LBF assemblages occur at ~18.6 m of the section (Fig. 4). Below ~18.6 m of the section, the LBF assemblage mainly consists of *Miscellanea miscella*, *Ranikothalia nuttalli*, *Lockhartia conditi*, *L. haimei*, *Kathina nammalensis*, and *Operculina* sp., indicating a paleowater depth of ~40–80 m (Hottinger 1997). Immediately above ~18.6 m, these LBF are replaced by porcellaneous-walled *Orbitolites* sp., *Alveolina subsolanus*, *A. agerensis*, and *A. ellipsoidalis* (Zhang et al. 2019). In the Tethyan shallow benthic zonation (SBZ), co-occurrence of *M. miscella* and *R. nuttalli* suggests the SBZ5 and the existence of *A. ellipsoidalis* indicates the SBZ6 (Serra-Kiel et al. 1998). By following correlation schemes between the Tethyan SBZ and plankton biozonations (Papazzoni et al. 2017; Serra-Kiel et al. 1998), SBZ5 corresponds to the P5b in planktonic foraminiferal zones and the NP9b in calcareous nannofossil zones, in which the PETM-CIE occurred (Dupuis et al. 2003). Thus, we confirm that section 13ZS covers the key stratigraphic interval of the uppermost Paleocene and the lowermost Eocene (Zhang et al. 2019). Based on a previously published bulk-carbonate $\delta^{13}C$ record (Zhang et al. 2017), the CIE interval in section 13ZS is positioned between stratigraphic levels of the CIE onset at 7.6 m and the $\delta^{13}C$ minimum at 18.4 m in this section (Fig. 4).

In this study, geochemical analyses are mainly conducted on LBF shells. LBF are an informal group of benthic foraminifera that are larger than 1 mm in diameter and host symbiotic algae (Hallock and Glenn 1986). They inhabit the photic zone of the ocean, thriving in shallow, warm, oligotrophic marine environments and having lifespans of several months to several years (Beavington-Penney and Racey 2004). Eutrophication is immediately fatal for the symbiont-bearing LBF (Hottinger 1998). Our studied *Miscellanea*, *Operculina*, and *Lockhartia* have hyaline lamella-perforate shells. Compared with planktonic foraminiferal shells, LBF shells are larger and thicker. They contain structural elements that are less porous or even imperforate (*e.g.*, pillars, piles, septa, some parts of chamber walls) (Hottinger 2006; Leppig 1988), and these elements proved suitable for *in situ* $\delta^{13}C$ measurements by SIMS (Figs. 5B–D, 6).

2.1. *In situ* $\delta^{13}C$ measurements

Selected samples were cut into ~1-mm thick chips using a jeweler's saw with a small-kerf diamond-embedded blade. About 5–6 chips and 2–3 grains of the UWC-3 calcite standard ($\delta^{13}C = -0.91 \pm 0.04$‰, VPDB, Kozdon et al. 2009) were cast in a 25-mm diameter epoxy mount. In each epoxy mount, all chips and calcite standard grains were placed within 8 mm of the center to minimize instrumental bias caused by sample position (Valley and Kita 2009). The surface of epoxy mounts was polished to a relief of < 1 μm and coated with a thin layer of gold (~50 nm) for SIMS measurements. *In situ* $\delta^{13}C$ measurements were carried out on a CAMECA IMS-1280 large radius multicollector SIMS at the WiscSIMS Laboratory, Department of Geoscience, University of Wisconsin-Madison. Two sessions were performed with session 1 on the date of 8/21/2017 and session 2 on the date of 9/14/2017 (see Supplementary data for details). The $^{133}Cs^+$ primary beam of 10 kV and 0.6 nA was focused to an 8 μm diameter spot size on the sample surface, sputtering secondary ions and etching ~1 μm deep pits. The secondary $^{12}C^-$, $^{13}C^-$ and $^{13}CH^-$ ions were collected simultaneously by using one Faraday cup (L'2) and two electron multipliers (axial and H2), respectively. The count rate for $^{12}C^-$ ions was ~7×10^6 cps. Each measurement lasted ~5 min, including 20 s of pre-sputtering, 60 s of automatic centering secondary ion beam in the field aperture and optimizing its transmission into mass spectrometer, and 160 s of collection of secondary ion signals. Groups of 10–16 spot analyses in samples were bracketed by 8 spot measurements on the standard grain in order to

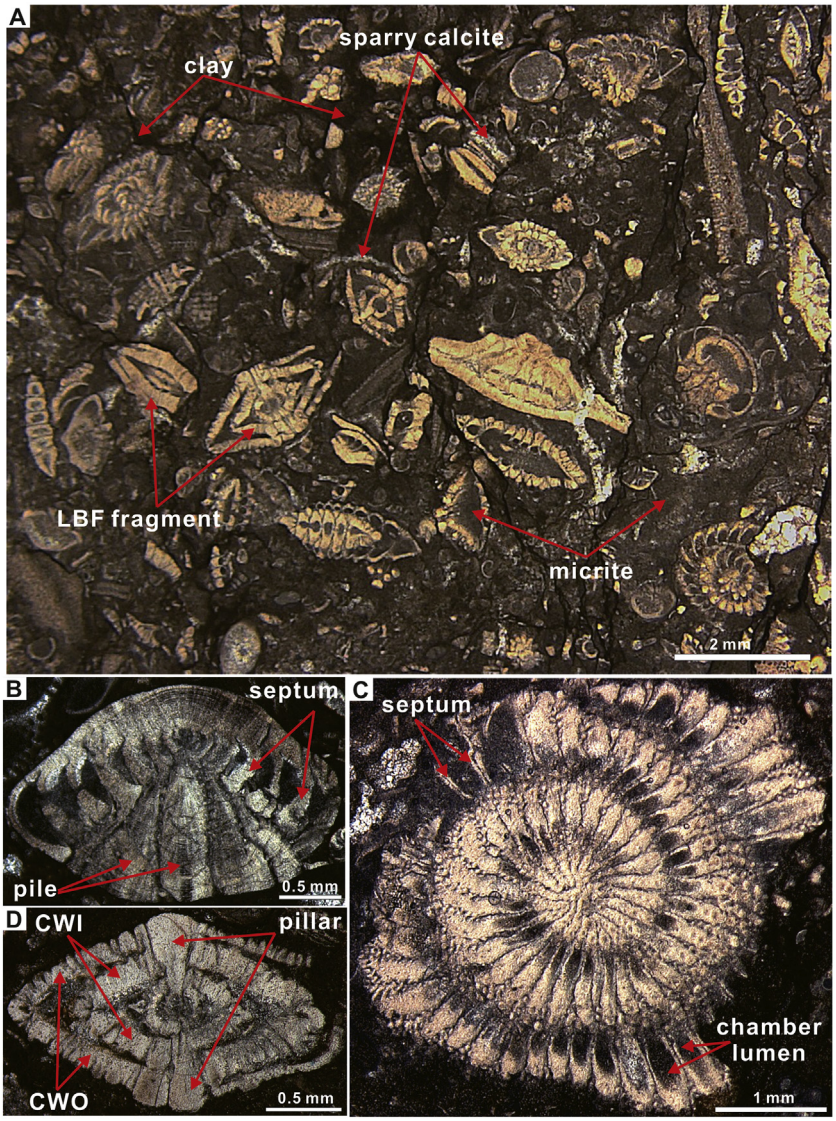

Fig. 5. Thin-section microphotographs showing major components in samples from section 13ZS at Tingri (south Tibet) and illustrating LBF structural elements analyzed by SIMS. (A) Microphotograph showing the dominant components of LBF fragments and micrites with minor sparry calcites and clay. (B) *Lockhartia*, axial section. (C) *Miscellanea*, equatorial section. (D) *Miscellanea*, axial section. CWI: chamber wall in the inner whorl; CWO: chamber wall in the outer whorl.

determine instrumental mass fractionation corrections for sample measurements. The external precision for sample measurements is the reproducibility of 8 measurements on standard grain that bracket each set of sample measurements, and the precision ranges from ± 0.42‰ to ± 0.98‰ at 2 standard deviations (SD). All pits left by SIMS analysis were examined by SEM, and *in situ* $\delta^{13}C$ data from pits with irregular shapes, intersecting cracks, or contaminated by epoxy were omitted.

2.2. Micro-analytical geochemical analyses

Contents of Ca, Sr, Al, Mn, Y, La, and Ce were measured on thin sections using LA-ICPMS at the Department of Geosciences, University of Bremen. The instrument is a high-resolution double-focusing Thermo Finnigan Element 2 coupled to a New Wave UP193ss laser ablation system with a wavelength of 193 nm. Helium and argon were used as carrier and make-up gas, respectively. Plasma power was 1200 W. Samples and standard materials were ablated with a laser fluence of 2.5 J/cm^2, a pulse rate of 5 Hz, and a spot diameter of 75 μm. No interference corrections were applied because formation of oxides in the plasma was low (ThO/Th ≤ 0.15%). NIST610 glass was analyzed as external calibration standard for every 10 samples. The Cetac GeoPro™ software was used for data quantification, with ^{43}Ca as internal standard. Data quality was assessed by repeated analyses of USGS reference materials BHVO2G, BCR2G (basalt glasses), and MACS3 (carbonate) along with the samples. The mean deviation from the reference values (GeoReM data base, MPI Mainz) is < 10%, and external precision at the 1 μg/g level is better than 5%, as determined by consecutive analyses of NIST614 glass.

3. Results and discussion

3.1. Diagenetic evaluation

Evaluating diagenetic effects on element concentrations and isotope compositions of ancient shallow-marine carbonate sediments/rock is one of the most vexing problems in paleoclimatic studies. Most, if not all, carbonate sediments/rock have undergone varying degrees of diagenetic alterations. However, the extent to which diagenesis has affected these primary geochemical signals is widely debated (Ahm et al. 2018; Banner and Hanson 1990; Brand and Veizer 1980, 1981; Denison et al. 1994; Derry et al. 1992; Derry 2010; Derry et al. 1992; Halverson et al. 2002, 2005, 2007; Higgins et al. 2018; Husson et al. 2015;

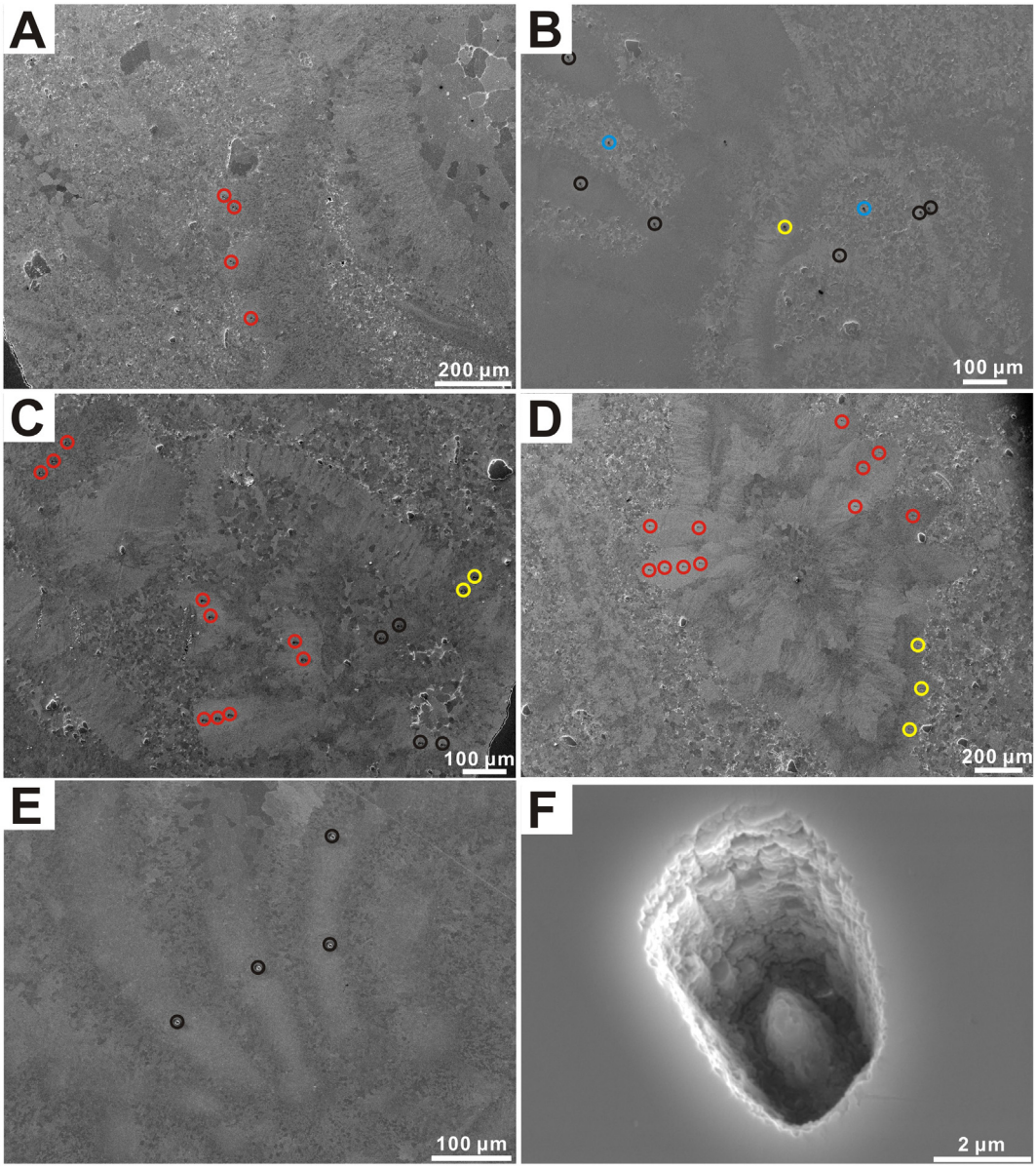

Fig. 6. SEM images showing locations of SIMS $\delta^{13}C$ analysis pits in (A) pillars of *Miscellanea* at 4.70 m of section 13ZS, (B) septa and chamber walls of *Operculina* as well as micrite filling chamber lumen at 7.55 m, (C) chamber wall, piles, and septa of *Lockhartia* and a pillar of *Miscellanea* at 9.90 m, (D) pillars and chamber wall in outer whorl of *Miscellanea* at 18.20 m, and (E) septa of *Miscellanea* at 18.40 m. (F) Highly magnified image showing the typical shape of a SIMS analysis pit. Circles refer to analysis pits in pillars/piles (red), septa (black), chamber walls (yellow), and micrite filling chamber lumens (blue). (For interpretation of the references to colour in this figure legend, the reader is referred to the web version of this article.)

Jacobsen and Kaufman 1999; Kaufman et al. 1991; Kaufman and Knoll 1995; Knauth and Kennedy 2009; Marshall 1992; Nabelek 1987; Swart and Eberli 2005; Swart and Kennedy 2012). A number of factors can dictate the ultimate chemical compositions of diagenetic carbonates, *e.g.*, carbonate mineralogy, fluid compositions, fluid/rock ratio, trace element distribution coefficients, isotopic fractionation factors. However, it generally agrees, or at least in many cases, that (1) increasing levels of diagenesis will lead to the gain of Mn and loss of Sr, and (2) the $\delta^{13}C$ is less susceptible to diagenetic alterations than the $\delta^{18}O$ and $^{87}Sr/^{86}Sr$, especially when diagenesis is related to fluid-rock interaction in a closed system (Ahm et al. 2018; Banner and Hanson 1990; Brand and Veizer 1980, 1981; Derry et al. 1992; Husson et al. 2015; Jacobsen and Kaufman 1999; Kaufman et al. 1991; Kaufman and Knoll 1995; Marshall 1992; Siahi et al. 2018). Our previous investigation on bulk carbonate from section 13ZS (Zhang et al. 2017) showed that (1) LBF fragments and micritic parts has very weak luminescence; (2) Bulk carbonate has relatively high Sr concentrations (mostly between 800 and 1400 ppm) and generally low Mn concentrations (~40–200 ppm, mostly < 70 ppm); (3) Mn/Sr ratios (< 0.2) in bulk carbonate are much lower than the empirical guideline (Mn/Sr < 1–2) indicative of good preservation of primary $\delta^{13}C$ signals in ancient carbonate rock; (4) No evident correlation between Mn/Sr ratios and $\delta^{13}C$ values can be observed in bulk carbonate; (5) $^{87}Sr/^{86}Sr$ ratios from bulk carbonate still preserve the primary signal of contemporary sea water in the open ocean. Taken together, these lines of evidence made us conclude that limestone samples from section 13ZS had experienced fluid-rock interaction in a closed system and the $\delta^{13}C$ of measured bulk carbonate (*i.e.*, micrites and LBF fragments) was largely unaltered by diagenesis.

In paleoclimatic studies, foraminifera with "glassy" shells are widely accepted as having preserved primary geochemical compositions, even for diagenesis-sensitive temperature proxies of $\delta^{18}O$ and Mg/Ca ratios (Pearson et al. 2001; Sexton et al. 2006). A previous study suggested

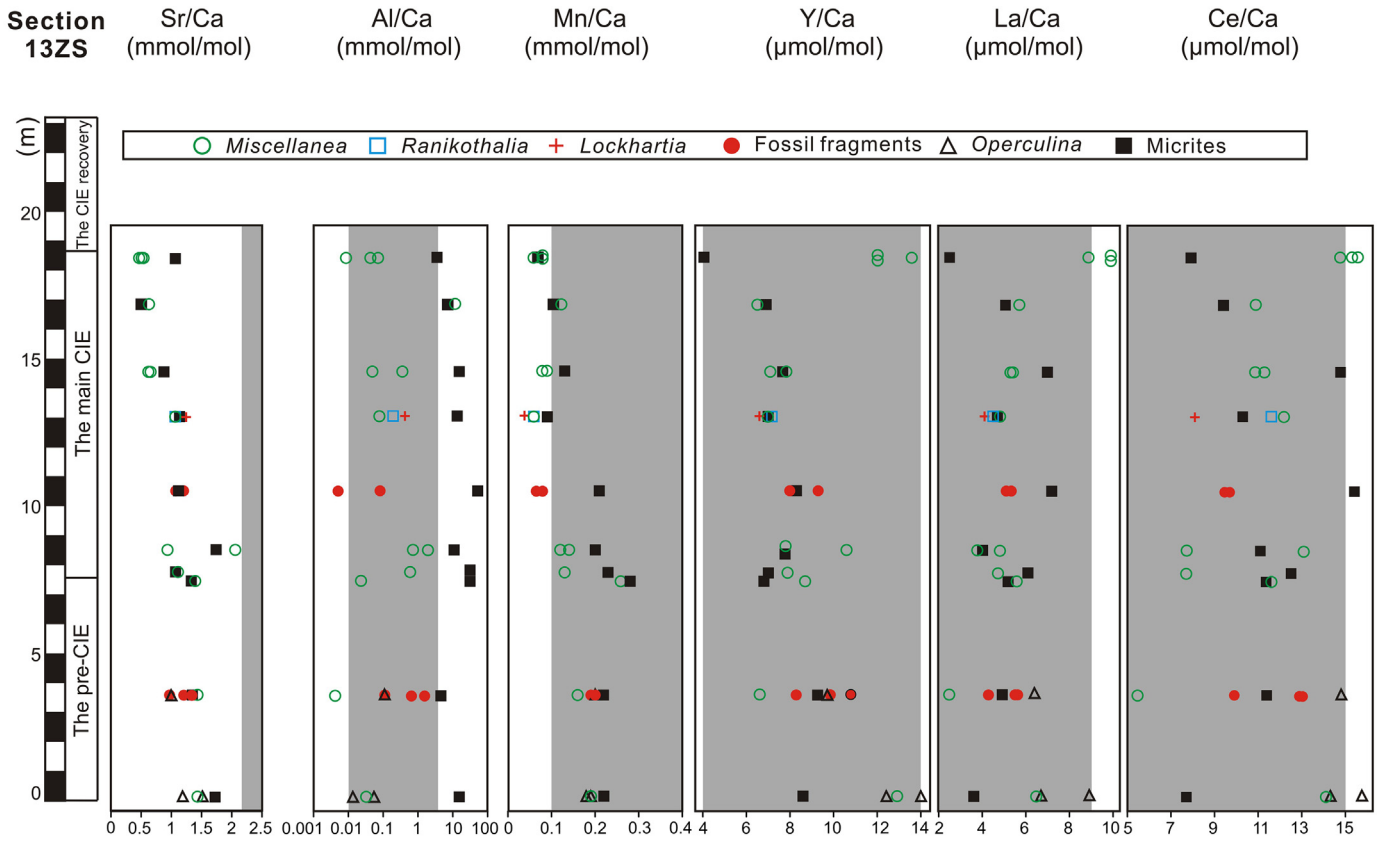

Fig. 7. Element/Ca ratios from section 13ZS. Grey shading highlights ranges of element/Ca ratios from Eocene-aged LBF with glassy shells (Evans et al. 2013). Note that Al/Ca ratios are plotted with a logarithmic scale.

that some Eocene LBF (*Operculina*, *Nummulites*) with "glassy" shells preserved primary Mg/Ca ratios (Evans et al. 2013). A corollary to this conclusion is that the primary $\delta^{13}C$ signal should have also been preserved in these Eocene "glassy" LBF, because the $\delta^{13}C$ is more resistant to diagenesis than both $\delta^{18}O$ and Mg/Ca ratios (Sexton et al. 2006). In the following, we take ratios of Sr/Ca, Al/Ca, Mn/Ca, Y/Ca, La/Ca, and Ce/Ca of these Eocene "glassy" LBF as guidelines to re-evaluate possible diagenetic effects on the LBF $\delta^{13}C$ from section 13ZS.

We analyze *in situ* values of Sr/Ca, Al/Ca, Mn/Ca, Y/Ca, La/Ca, and Ce/Ca of LBF shells and micrites in section 13ZS (Fig. 7). Sr/Ca ratios from LBF and micrites vary between ~0.4–2.1 mmol/mol, which are lower than those (~2.2–2.7 mmol/mol) from modern *Operculina* and Eocene glassy LBF (Evans et al. 2013). Increasing level of diagenesis can reduce Sr/Ca ratios in foraminiferal shells (Kozdon et al. 2013). However, a number of other variables may also affect the Sr/Ca ratios, such as temperature, salinity, pH, carbonate ion concentration, and Sr/Ca ratio of contemporary seawater as well as shell size (Dissard et al. 2010; Keul et al. 2017; Kozdon et al. 2013; Lea et al. 1999; Yu et al. 2014). In spite of possible effects from these variables, we tend to interpret the Sr/Ca ratios in section 13ZS as being affected by diagenesis. However, the existence of diagenetically altered Sr/Ca does not necessarily imply that the primary $\delta^{13}C$ must also be significantly altered. A numerical model of shallow-marine carbonate diagenesis suggested that in sediment-buffered conditions (a closed system with respect to carbon) the $\delta^{13}C$ was nearly unaffected by diagenesis, irrespective of cumulative fluid-rock ratios. With respect to Sr/Ca ratios, however, they started to decline as cumulative fluid-rock ratios reached to $\sim 10^2$. Comparatively, $^{87}Sr/^{86}Sr$ ratios were more diagenetically resistant than Sr/Ca ratios, and the $^{87}Sr/^{86}Sr$ could retain its primary signal until cumulative fluid-rock ratio reached to $\sim 2 \times 10^4$ (Ahm et al. 2018 and its Supplementary information). Combined with this modeling study, our published $^{87}Sr/^{86}Sr$ data and Sr/Ca ratios, we infer that diagenesis in section 13ZS, likely with cumulative fluid-rock ratios of $\sim 10^2$–10^4 in a closed system, has altered primary Sr/Ca ratios, but left the $\delta^{13}C$ and $^{87}Sr/^{86}Sr$ largely unaffected.

In section 13ZS, Al/Ca ratios from LBF and micrites are ~0.01–2 mmol/mol and ~4–50 mmol/mol, respectively. The former agrees well with those (0.01–4 mmol/mol) from modern and Eocene glassy LBF (Evans et al. 2013), indicating negligible effects from clay contamination. However, evidently higher Al/Ca values in micrites suggest presence of a certain amount of clay minerals. Trace elements of Mn, Y, La, Ce in foraminifer calcite can be used to evaluate diagenetic effects, among which Mn is the most reliable diagenetic proxy (Lea 1999). Generally, ratios of Mn/Ca, Y/Ca, La/Ca, and Ce/Ca in foraminifer calcite will increase as the degree of diagenetic alteration increases (Evans et al. 2013; Lea 1999). Modern *Operculina* specimens from neritic environments typically register characteristic Mn/Ca ratios of ~0.004–0.1 mmol/mol, and the Eocene specimens of *Nummulites* and *Operculina* with glassy shells show higher Mn/Ca ratios of ~0.1–0.4 mmol/mol (Evans et al. 2013). We therefore consider Mn/Ca ratios < 0.4 mmol/mol as indicating preservation of primary shell chemistry in fossilized LBF. In section 13ZS, Mn/Ca ratios of LBF shells and micrites range from 0.05 mmol/mol to 0.3 mmol/mol, with most of the ratios being < 0.2 mmol/mol. The difference in Mn/Ca ratios between co-occurring LBF shells and micrites is small, and Mn/Ca ratios within the CIE interval are slightly lower than those from pre-CIE materials (Fig. 7). The ratios of Y/Ca, La/Ca, and Ce/Ca cluster around ~6–12 μmol/mol, ~4–8 μmol/mol, and ~7–14 μmol/mol, respectively, and there are no clear stratigraphic trends among these elemental ratios (Fig. 7). Although these ratios are ~10× higher than those from modern *Operculina* specimens, they are very similar to those of Eocene "glassy" LBF (Evans et al. 2013). Consistency of these element/Ca distributions between LBF from section 13ZS and the Eocene "glassy" LBF suggests that diagenesis very likely had an insignificant effect on the

preservation of the primary $\delta^{13}C$ signal in LBF shells from section 13ZS.

Except for aforementioned geochemical evidence, another line of argumentation for the primary $\delta^{13}C$ signal in section 13ZS is global spatial reproducibility of the stepped CIE (Fig. 3). Although increased meteoric diagenesis associated with sea level fall was proposed to have caused a contemporary $\delta^{13}C$ decrease from some widely separated, shallow-marine, Pliocene-Pleistocene carbonate sections (Swart and Kennedy 2012), this mechanism may be irrelevant to the formation of the stepped CIE during the PETM. Owing to thermal expansion of seawater and/or melting of small alpine ice sheets (Sluijs et al. 2008), sea level was rising during the PETM, instead of falling. This will reduce the possibility of subaerial exposure and/or exposure to meteoric lenses, thus alleviating meteoric diagenesis in shallow-marine carbonate platforms/ramps. Besides, the stepped CIE during the PETM is recognized not only from the shallow-marine carbonate section at Tingri, but also from a lacustrine section in the Nanyang Basin and several hemipelagic/pelagic sections (Mead Stream, ODP Sites 689 and 690), likely also from the paleosol record in the Bighorn Basin (Bains et al. 2003). Thus, we cannot ascribe the stepped CIE preserved in these different depositional environments to diagenetic processes, including meteoric diagenesis. Instead, we may interpret the stepped CIE as representing the fidelity of carbon perturbations during the PETM, with negligible diagenetic alterations.

3.2. The $\delta^{13}C$ of different carbonate components

We measured *in situ* $\delta^{13}C$ of different carbonate components from seven limestone samples. In section 13ZS, these samples were situated at the depths of 4.70 m, 7.55 m, 7.90 m, 9.90 m, 15.45 m, 18.20 m, and 18.40 m, respectively. (Fig. 4). Two samples at 4.70 m and 7.55 m are located within the pre-CIE interval (Fig. 8A & B), and the rest are from the CIE interval (Fig. 8C–G). The sample at 18.40 m documents the most negative $\delta^{13}C$ value during the PETM (Fig. 8G).

In situ $\delta^{13}C$ measurements show that intra-shell $\delta^{13}C$ variability in shells of *Miscellanea* and *Lockhartia* is very limited (Fig. 8A & C) or slightly evident (Fig. 8D–G), and that $\delta^{13}C$ values measured from these two genera are indistinguishable (Fig. 8D). In contrast, *Operculina* exhibits a systematic intra-shell $\delta^{13}C$ variation where $\delta^{13}C$ values of chamber walls and septa in the inner whorl are ~0.9‰ lower than those in the outer whorl (Fig. 8B). Micrite $\delta^{13}C$ roughly co-varies with LBF shell $\delta^{13}C$ (Fig. 8B, E & G), exhibiting a large decline across the CIE onset (Fig. 8E & G). Except for the sample at 4.70 m, bulk carbonate $\delta^{13}C$ values in the remaining samples are very close to average $\delta^{13}C$ values of LBF shells from the same stratigraphic sample (Fig. 8).

Although it remains unclear whether vital effects have influenced the $\delta^{13}C$ compositions of *Miscellanea* and *Lockhartia*, the limited intra-shell and inter-genus $\delta^{13}C$ variations registered by these two taxa suggest that the $\delta^{13}C$ of their shells are mainly controlled by the $\delta^{13}C$ of dissolved inorganic carbon in ambient seawater. With respect to *Operculina*, however, the increase in shell $\delta^{13}C$ values towards the outer whorl indicates that, in addition to the seawater $\delta^{13}C$, some physiological processes, such as symbiont photosynthesis, may have affected the shell $\delta^{13}C$ (*e.g.*, Spero et al. 1991).

Micrites in shallow-marine limestone have multiple sources; nevertheless, the $\delta^{13}C$ similarity between micrites and LBF indicates that micrites may result from physical or biological abrasion/disintegration of skeletal materials, such as LBF shells. Alternatively, micrites could be a result of cementation during early marine burial diagenesis (Munnecke et al. 1997). In this case, cementation in section 13ZS should have been completed within ~1–2 kyr after the deposition of biogenic clasts so that the chemistry of diagenetic fluid is still modulated by contemporary seawater. The rapid completion of cementation can be inferred from the SIMS $\delta^{13}C$ data at ~7.55 m (Fig. 8B) and at ~7.90 m (Fig. 8C). In section 13ZS, the large $\delta^{13}C$ decrease from ~7.55 m to ~7.90 m represents the CIE onset (phase **c** in the stepped CIE), and the duration of phase **c** was suggested to be ~1–2 kyr according to ^{3}He and orbital age models at ODP Site 690 (Farley and Eltgroth 2003; Röhl et al. 2007). Apparently, the micrite $\delta^{13}C$ from the sample at ~7.55 m was not affected by the subsequent large decrease in seawater $\delta^{13}C$ at ~7.90 m, indicating that cementation in the sample at ~7.55 m should have been completed prior to deposition of the sample at ~7.90 m. This inference is compatible with previous studies of carbonate-sediment lithification in modern shallow-marine environments, which reported that Holocene sediments were cemented within several tens of years, with average cement growth rates of ~8–10 cm/kyr (Grammer et al. 1993). Rapid cementation would decrease porosity and permeability in carbonate sediments quickly, thereby inhibiting further diagenesis and allowing cements to preserve the isotopic composition of contemporary seawater. In section 13ZS, bulk carbonate mainly consists of micrites and LBF fragments, and these two carbonate components have similar $\delta^{13}C$ values (Fig. 8B, E & G). We therefore attribute the similar $\delta^{13}C$ values returned by bulk carbonate and LBF shells from the same stratigraphic sample to rapid cementation.

3.3. The CIE magnitude in the surface ocean

In section 13ZS, the new SIMS data show that *Miscellanea* at 18.40 m records the most negative $\delta^{13}C$ value during the PETM (mean $\delta^{13}C = -4.3‰$) and *Operculina* at 7.55 m registers the latest pre-CIE $\delta^{13}C$ value (mean $\delta^{13}C = 3.0‰$). The difference in the average SIMS $\delta^{13}C$ values between them is ~7.3‰. Since it is still uncertain whether inter-genus $\delta^{13}C$ variability exists between *Miscellanea* and *Operculina*, we constrain the CIE magnitude using the SIMS $\delta^{13}C$ value of *Miscellanea* at 4.70 m and obtain an average CIE magnitude of ~7.2‰. In the box and whisker plot generated with SIMS data (Fig. 9), the CIE magnitude is suggested to be ~7‰ or ~7.3‰. Thus, the CIE magnitude from foraminiferal shells (~7–7.3‰) is very similar to the CIE magnitude from bulk carbonate in the same section (~7‰) (Zhang et al. 2017).

Some studies found that elevated warming and ocean acidification can lead to partial or complete loss of symbionts in some LBF species, which will inhibit symbiont activities and cause “bleaching” in the LBF (Schmidt et al. 2011, 2014; Talge and Hallock 2003). Symbiont activities can increase the $\delta^{13}C$ of foraminiferal shell *via* preferentially utilizing ^{12}C-enriched CO_2 (Spero et al. 1991). If LBF bleaching did happen during the PETM and if vital effects of *Miscellanea* $\delta^{13}C$ in the Paleocene were not trivial, the ~7‰ CIE magnitude from SIMS measurements could be amplified by changes in *Miscellanea* physiology during the PETM. However, based on our SIMS data, *Miscellanea* does not show systematic variations in $\delta^{13}C$ from their inner whorl to outer whorl (Fig. 8C, G), although *Operculina* exhibits an evident $\delta^{13}C$ increase towards their outer whorl (Fig. 8B). Thus, we tentatively infer that, compared with *Operculina*, carbon isotope vital effects in *Miscellanea* might be very small during the PETM. If true, the assumed physiological effect on the CIE magnitude from section 13ZS will be insignificant.

At ODP Site 690, the CIE magnitude based on single-shell $\delta^{13}C$ data from mixed-layer foraminifera is ~4‰ (Zachos et al. 2007), which is evidently smaller than the ~7‰ CIE magnitude at Tingri. Two potential factors, incomplete preservation and diagenesis, could attenuate the CIE magnitude at this Site. As noted above, carbonate dissolution did happen at ODP Site 690, and it should have affected mixed-layer foraminifera more severely than coccoliths and other foraminifera. Thus, the PETM-CIE record registered by planktonic foraminiferal at this site is likely incomplete. Although the effect of incomplete preservation on the foraminiferal CIE magnitude cannot be readily quantified, it might have decreased its size to some extent. Besides, Kozdon et al. (2018) found that, at ODP Site 865 where the full CIE was not preserved, the SIMS-derived CIE magnitude (~4.6‰) from preserved foraminiferal records was evidently larger than the magnitude from single-shell $\delta^{13}C$ data (~3.1‰), and the latter was suggested to have been attenuated by involvement of diagenetic crystallites and calcite infilling. The diagenetic calcite was formed during the CIE recovery and had $\delta^{13}C$ values

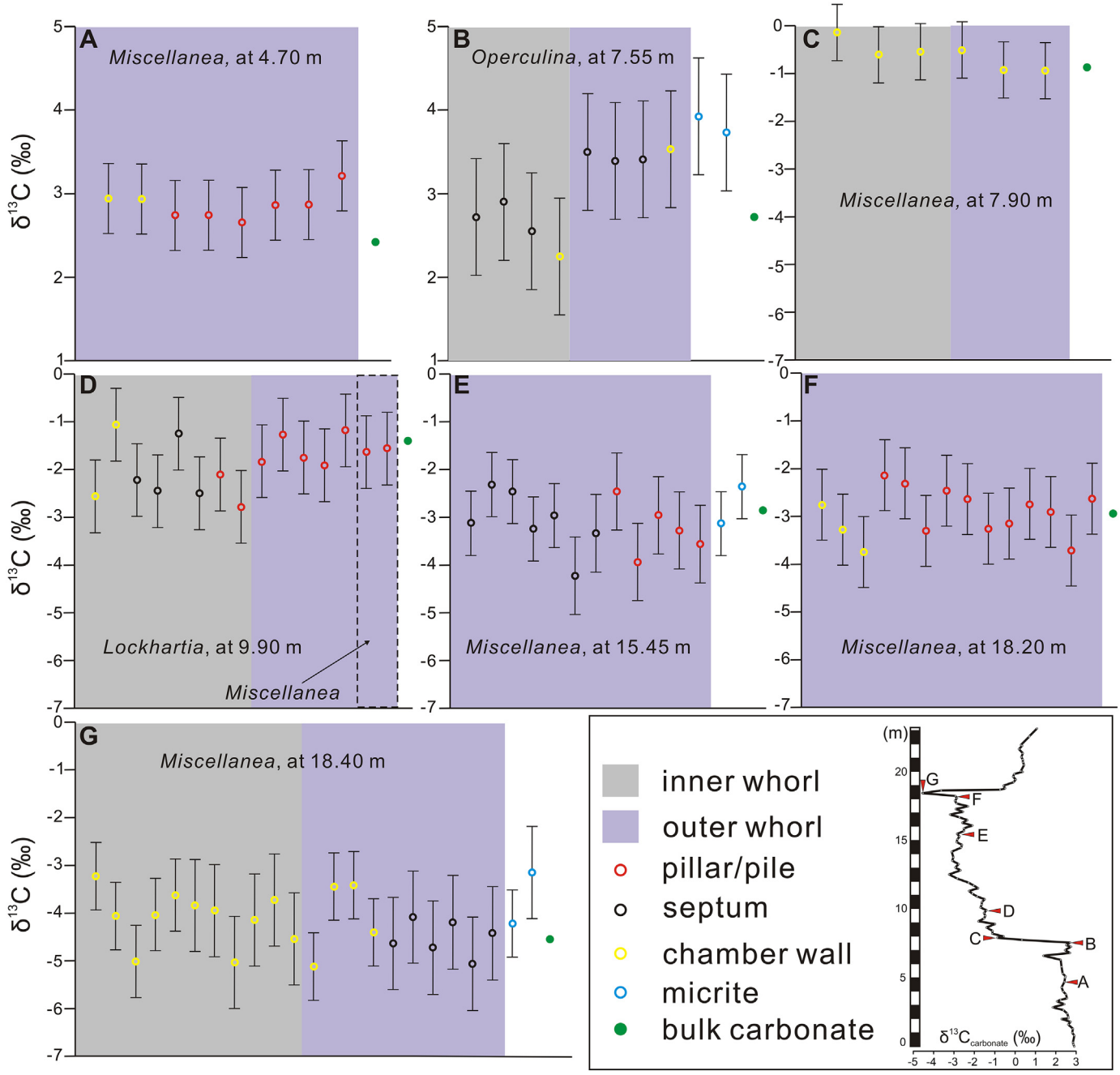

Fig. 8. Intra-shell $\delta^{13}C$ variability delineated by series of *in situ* SIMS analyses taken from pillar/pile, septum, chamber wall of LBF shells from pre-CIE (A-B) and CIE (C-G) samples of section 13ZS. Correlative $\delta^{13}C$ values of micrite and bulk carbonate are also shown for comparison. The $\delta^{13}C$ values with error bars are obtained from *in situ* SIMS measurements (this study), and the $\delta^{13}C$ of bulk carbonate was measured using conventional isotope ratio mass spectrometry (Zhang et al. 2017). Note the CIE onset (phase **c** in the stepped CIE) is constrained by initial $\delta^{13}C$ decrease between ~7.55 m and ~7.90 m, and the negative CIE terminates at ~18.40 m of section 13ZS. Error bars denote two standard deviations. Symbols and stratigraphic positions of SIMS-analyzed samples are shown in the inset figure.

falling between those of pre-CIE and CIE foraminiferal shells (Kozdon et al. 2018). The existence of diagenetic crystallites in both pre-CIE and CIE foraminiferal specimens will decrease their pre-CIE values and increase CIE values measured from single-shell foraminifera, thus shrinking the true CIE magnitude. This diagenesis-induced attenuation probably occurs in most (if not all) pelagic PETM sections and SIMS analysis of foraminiferal shells from ODP Site 690 might provide a better constraint on the true CIE magnitude in the surface ocean.

In a review paper, McInerney and Wing (2011) compiled 48 published terrestrial CIE records with the magnitude ranging from 2.2‰ to 7.6‰ and took their median value of 4.6‰ as representing the CIE magnitude in the atmosphere. To our knowledge, except for the paleosol record at Polecat Bench in the Bighorn Basin, most of other terrestrial records in their compilation are stratigraphically incomplete and probably fail to preserve their full CIE. In this case, we suggest that the maximum value (7.6‰) of the CIE magnitude from their compilation, instead of the median value, may better reflect the full extent of carbon perturbations in the atmosphere. We note that their compilation of CIE magnitude from planktonic foraminifera can lend support to this suggestion. McInerney and Wing (2011) also compiled 36 planktonic foraminiferal CIE records, and obtained a median value of 2.6‰ and a maximum value of 4.4‰. Similar to the terrestrial records, these foraminiferal records largely preserve a fragmentary CIE history owing to carbonate dissolution on the deep-sea floor. As discussed above, the CIE

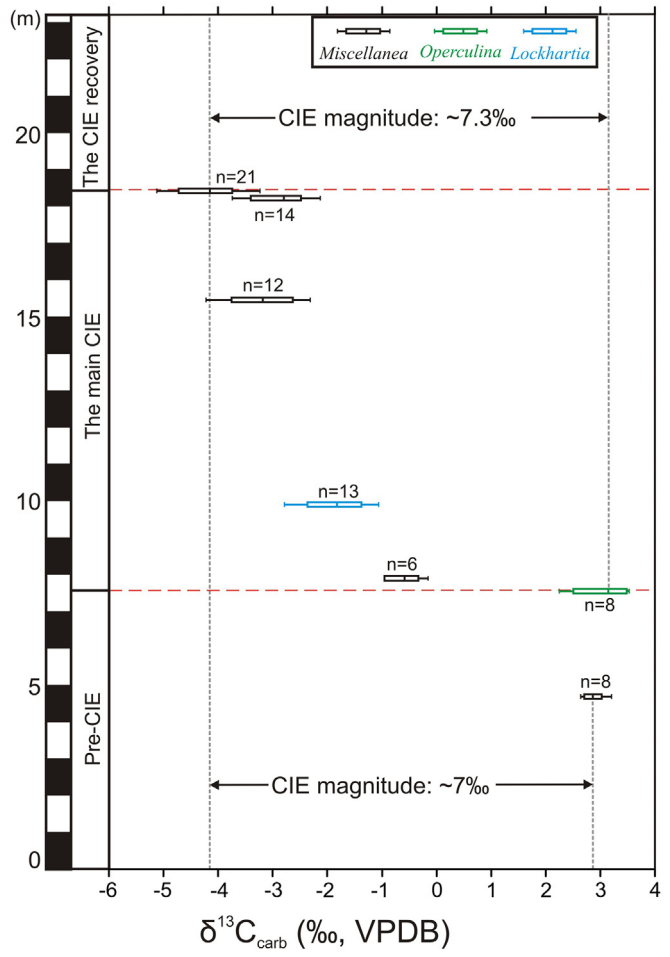

Fig. 9. Box and whisker plot illustrating the CIE magnitude registered by LBF shells from section 13ZS. Boxes represent the first and third quartiles of SIMS $\delta^{13}C$ values from analyzed LBF shells, and vertical lines within boxes denote the median values. Whiskers show the minimum and maximum $\delta^{13}C$ values. Two red dashed lines delimit the CIE interval in section 13ZS. (For interpretation of the references to colour in this figure legend, the reader is referred to the web version of this article.)

magnitude in mixed-layer planktonic foraminifera should be > 4–4.6‰ (Kozdon et al. 2018; Zachos et al. 2007). Thus, it is the maximum value (4.4‰) in their compilation, not the median value (2.6‰), that can better characterize the CIE magnitude registered by planktonic foraminifera. In terrestrial CIE records, we therefore prefer to take the value of 8‰ from paleosol CIE records in the Bighorn Basin as representing the full CIE magnitude in the atmosphere (Bains et al. 2003; Bowen et al. 2001), although it was suggested an increase in humidity might amplify the paleosol CIE records to some extant (Bowen et al. 2004).

During the PETM, a significant quantity of ^{13}C-depleted carbon was released into the atmosphere (Bowen et al. 2001; Thomas et al. 2002), and the released carbon should have affected the surface ocean through air-sea CO_2 exchange. Mixing time for carbon exchange between atmosphere and surface ocean is decades (Rohling et al. 2012), which is short enough for $\delta^{13}C$ in the atmosphere and surface ocean to equilibrate. Thus, both atmosphere and the surface ocean should record the similar CIE magnitude during the PETM. This inference is generally supported by previous studies and our work from Tingri. Based on SIMS analysis of planktonic foraminifera at ODP Site 865, Kozdon et al. (2018) inferred the actual size of the CIE in the surface ocean might be on the order of ~5–6‰. Besides, the paleosol CIE records in the Bighorn Basin suggested that the CIE magnitude in the atmosphere was ~8‰ (Bains et al. 2003; Bowen et al. 2001). Our work at Tingri indicates that the CIE magnitude in the surface ocean is ~7‰. Collectively, these studies show that the $\delta^{13}C$ in the atmosphere and surface ocean may have decreased by ~7‰ during the PETM.

3.4. Constraint on the mass of the released carbon during the PETM

It was generally agreed that thousands of petagrams of ^{13}C-depleted carbon had been added into the atmosphere-ocean system during the PETM. However, estimates of the carbon mass from different studies varied greatly. For example, Zachos et al. (2005) estimated that > 4500 Pg C was required to shoal calcite compensation depth (CCD) to < 1 km water depth in much of the ocean during the PETM. Later, this number was enlarged to > 6800 Pg C using GENIE-1 model (Panchuk et al. 2008). Zeebe et al. (2009), employing a carbon cycle model LOSCAR, suggested that an initial pulse of 3000 Pg C with a subsequent bleeding of ~1480 Pg C (with the $\delta^{13}C < -50‰$) could reproduce the extent of CCD shoaling and the CIE magnitude. Using UVic Earth System Climate Model simulations, Meissner et al. (2014) found that a release of 7000–10,000 Pg C into the ocean-atmosphere system agreed best with temperature reconstructions. Recently, Gutjahr et al. (2017) proposed that the carbon mass might have exceeded 10,000 Pg C by using cGENIE model to simulate the observed pH decline and the CIE magnitude. In this study, we propose that the CIE magnitude in the surface ocean and atmosphere is ~7‰, which is significantly larger than previous expected. If we consider ~7‰ CIE as representing the full extent of the $\delta^{13}C$ decline in the atmosphere-ocean system, simple mass balance calculations, based on the equation from McInerney and Wing (2011), yield ~7000 Pg C from methane hydrate (with the $\delta^{13}C$ of −60‰) or ~28,000 Pg C from organic matter (with the $\delta^{13}C$ of −22‰). However, we note that the reported largest CIE magnitude from benthic foraminifera is ~3.5‰ at ODP Site 1263 (McCarren et al. 2008) and thus think that the CIE magnitude in the deep ocean is probably less than ~7‰. So, we may consider ~28,000 Pg C as representing the upper end of the released carbon mass during the CIE, given that the carbon is sourced from organic matter, permafrost, thermogenic methane, methane hydrate, or any of their combinations.

4. Conclusions

In this study, we constrained the CIE magnitude in a tropical shallow-marine limestone succession (section 13ZS at Tingri, Tibet) using *in situ* $\delta^{13}C$ analyses by SIMS on micrometer-scale (~8 μm) domains in individual shells of larger benthic foraminifera (LBF). The CIE magnitude revealed by *in situ* $\delta^{13}C$ data from LBF shells is ~7‰ and compatible with that measured from some terrestrial PETM records, suggesting that both the atmosphere and the surface ocean had similar CIE magnitude (~7‰) during the PETM. Mass balance calculations indicate that the required carbon mass during the CIE interval would not exceed ~28,000 Pg, given that the carbon was released from organic matter, permafrost, thermogenic methane, methane hydrate, or any of their combinations. Our study also demonstrates that the $\delta^{13}C$ of some limestone sections formed on ancient shallow-marine carbonate ramps can avoid strong diagenetic overprinting and preserve true signals of deep-time carbon perturbations.

Declaration of Competing Interest

None.

Acknowledgements

We thank Peter Sadler for sharing his database, Anne Hübner and Patrick Monien for technical help in the laboratory. Two anonymous reviewers and the editor provided constructive comments, which improved the manuscript. We express our sincere gratitude to D. Clay

Kelly for discussion and valuable scientific input. Funding for this research was provided by grants from the National Natural Science Foundation of China (41490615), the Second Tibetan Plateau Scientific Expedition and Research (STEP) program (2019QZKK0708), National Key Research and Development Plan (2016YFC0600303), CAS Pioneer Hundred Talents Program, and the Deutsche Forschungsgemeinschaft (No. Wi725/29). WiscSIMS is supported by the U.S. National Science Foundation (EAR-1355590, 1658823) and the University of Wisconsin-Madison. John Valley is also funded by the U.S. Department of Energy (DE-FG02-93ER14389).

Appendix A. Supplementary data

Supplementary data to this article can be found online at https://doi.org/10.1016/j.gloplacha.2019.103049.

References

Ahm, A.-S.C., Bjerrum, C.J., Blättler, C.L., Swart, P.K., Higgins, J.A., 2018. Quantifying early marine diagenesis in shallow-water carbonate sediments. Geochim. Cosmochim. Acta 236, 140–159. https://doi.org/10.1016/j.gca.2018.02.042.

Andrews, E., White, T., del Papa, C., 2017. Paleosol-based paleoclimate reconstruction of the paleocene-eocene thermal maximum, northern argentina. Palaeogeogr. Palaeoclimatol. Palaeoecol. 471, 181–195. https://doi.org/10.1016/j.palaeo.2017.01.042.

Bains, S., Corfield, R.M., Norris, R.D., 1999. Mechanisms of climate warming at the end of the Paleocene. Science 285 (5428), 724–727. https://doi.org/10.1126/science.285.5428.724.

Bains, S., Norris, R.D., Corfield, R.M., Bowen, G.J., Gingerich, P.D., Koch, P.L., 2003. Marine-terrestrial linkages at the Paleocene-Eocene boundary. In: Wing, S.L., Gingerich, P.D., Schmitz, B., Thomas, E. (Eds.), Causes and Consequences of Globally Warm Climates in the Early Paleogene. 369. Geological Society of America Special Papers, Boulder, Colorado, pp. 1–9.

Banner, J.L., Hanson, G.N., 1990. Calculation of simultaneous isotopic and trace element variations during water-rock interaction with applications to carbonate diagenesis. Geochim. Cosmochim. Acta 54 (11), 3123–3137. https://doi.org/10.1016/0016-7037(90)90128-8.

Beavington-Penney, S.J., Racey, A., 2004. Ecology of extant nummulitids and other larger benthic foraminifera: applications in palaeoenvironmental analysis. Earth-Sci. Rev. 67 (3–4), 219–265. https://doi.org/10.1016/j.earscirev.2004.02.005.

Bolton, C.T., Stoll, H.M., 2013. Late miocene threshold response of marine algae to carbon dioxide limitation. Nature 500 (7464), 558–562. https://doi.org/10.1038/nature12448.

Bowen, G.J., Koch, P.L., Gingerich, P.D., Norris, R.D., Bains, S., Corfield, R.M., 2001. Refined isotope stratigraphy across the continental paleocene-eocene boundary on polecat bench in the Northern Bighorn Basin. In: Gingerich, P.D. (Ed.), Paleocene-Eocene Stratigraphy and Biotic Change in the Bighorn and Clarks Fork Basins, Wyoming. 33. University of Michigan Papers on Paleontology, Ann Arbor, pp. 73–88.

Bowen, G.J., Beerling, D.J., Koch, P.L., Zachos, J.C., Quattlebaum, T., 2004. A humid climate state during the palaeocene/eocene thermal maximum. Nature 432 (7016), 495–499. https://doi.org/10.1038/nature03115.

Bowen, G.J., Maibauer, B.J., Kraus, M.J., Rohl, U., Westerhold, T., Steimke, A., et al., 2015. Two massive, rapid releases of carbon during the onset of the palaeocene-eocene thermal maximum. Nat. Geosci. 8 (1), 44–47. https://doi.org/10.1038/ngeo2316.

Bralower, T.J., Kelly, D.C., Gibbs, S., Farley, K., Eccles, L., Lindemann, T.L., Smith, G.J., 2014. Impact of dissolution on the sedimentary record of the paleocene-eocene thermal maximum. Earth Planet. Sci. Lett. 401, 70–82. https://doi.org/10.1016/j.epsl.2014.05.055.

Bralower, T.J., Kump, L.R., Self-Trail, J.M., Robinson, M.M., Lyons, S., Babila, T., Ballaron, E., Freeman, K.H., Hajek, E., Rush, W., Zachos, J.C., 2018. Evidence for shelf acidification during the onset of the paleocene-eocene thermal maximum. Paleoceanography Paleoclimatol. 33, 1408–1426. https://doi.org/10.1029/2018PA003382.

Brand, U., Veizer, J., 1980. Chemical diagenesis of a multicomponent carbonate system-1: trace elements. J. Sediment. Petrol. 50 (4), 1219–1236. https://doi.org/10.1306/212F7BB7-2B24-11D7-8648000102C1865D.

Brand, U., Veizer, J., 1981. Chemical diagenesis of a multicomponent carbonate system-2: stable isotopes. J. Sediment. Petrol. 51 (3), 987–997. https://doi.org/10.1306/212F7DF6-2B24-11D7-8648000102C1865D.

Chiu, T.-C., Broecker, W.S., 2008. Toward better paleocarbonate ion reconstructions: new insights regarding the CaCO3 size index. Paleoceanography 23 (2), PA2216. https://doi.org/10.1029/2008PA001599.

Colosimo, A.B., Bralower, T.J., Zachos, J.C., 2006. Evidence for lysocline shoaling at the paleocene/eocene thermal maximum on shatsky rise, Northwest Pacific. In: Bralower, T.J., Premoli Silva, I., Malone, M.J. (Eds.), Proceedings of the Ocean Drilling Program, Scientific Results. 198. Ocean Drilling Program, Texas, pp. 1–36.

Denison, R.E., Koepnick, R.B., Fletcher, A., Howell, M.W., Callaway, W.S., 1994. Criteria for the retention of original seawater $^{87}Sr/^{86}Sr$ in ancient shelf limestones. Chem. Geol. 112 (1), 131–143. https://doi.org/10.1016/0009-2541(94)90110-4.

Derry, L.A., 2010. A burial diagenesis origin for the ediacaran Shuram-wonoka carbon isotope anomaly. Earth Planet. Sci. Lett. 294, 152–162. https://doi.org/10.1016/j.epsl.2010.03.022.

Derry, L.A., Kaufman, A.J., Jacobsen, S.B., 1992. Sedimentary cycling and environmental change in the late proterozoic: evidence from stable and radiogenic isotopes. Geochim. Cosmochim. Acta 56 (3), 1317–1329. https://doi.org/10.1016/0016-7037(92)90064-P.

Dickens, G.R., O'Neil, J.R., Rea, D.K., Owen, R.M., 1995. Dissociation of oceanic methane hydrate as a cause of the carbon isotope excursion at the end of the paleocene. Paleoceanography 10 (6), 965–971. https://doi.org/10.1029/95PA02087.

Diefendorf, A.F., Mueller, K.E., Wing, S.L., Koch, P.L., Freeman, K.H., 2010. Global patterns in leaf ^{13}C discrimination and implications for studies of past and future climate. Proc. Natl. Acad. Sci. 107 (13), 5738–5743. https://doi.org/10.1073/pnas.0910513107.

Dissard, D., Nehrke, G., Reichart, G.J., Bijma, J., 2010. The impact of salinity on the Mg/Ca and Sr/Ca ratio in the benthic foraminifera *Ammonia tepida*: results from culture experiments. Geochim. Cosmochim. Acta 74 (3), 928–940. https://doi.org/10.1016/j.gca.2009.10.040.

Dupuis, C., Aubry, M.-P., Steurbaut, E., Berggren, W.A., Ouda, K., Magioncalda, R., et al., 2003. The dababiya quarry section: lithostratigraphy, clay mineralogy, geochemistry and paleontology. Micropaleontology 49, 41–59. https://doi.org/10.2113/49.Suppl_1.41.

Evans, D., Müller, W., Oron, S., Renema, W., 2013. Eocene seasonality and seawater alkaline earth reconstruction using shallow-dwelling large benthic foraminifera. Earth Planet. Sci. Lett. 381, 104–115. https://doi.org/10.1016/j.epsl.2013.08.035.

Farley, K.A., Eltgroth, S.F., 2003. An alternative age model for the paleocene-eocene thermal maximum using extraterrestrial ^{3}He. Earth Planet. Sci. Lett. 208 (3–4), 135–148. https://doi.org/10.1016/S0012-821X(03)00017-7.

Grammer, G.M., Ginsburg, R.N., Swart, P.K., McNeill, D.F., Jull, A.J.T., Prezbindowski, D.R., 1993. Rapid growth rates of syndepositional marine aragonite cements in steep marginal slope deposits, Bahamas and Belize. J. Sediment. Petrol. 63 (5), 983–989. https://doi.org/10.1306/D4267C62-2B26-11D7-8648000102C1865D.

Gutjahr, M., Ridgwell, A., Sexton, P.F., Anagnostou, E., Pearson, P.N., Pälike, H., et al., 2017. Very large release of mostly volcanic carbon during the palaeocene–eocene thermal maximum. Nature 548 (7669), 573–577. https://doi.org/10.1038/nature23646.

Hallock, P., Glenn, E.C., 1986. Larger foraminifera: a tool for paleoenvironmental analysis of cenozoic carbonate depositional facies. Palaios 1 (1), 55–64. https://doi.org/10.2307/3514459.

Halverson, G.P., Hoffman, P.F., Schrag, D.P., Kaufman, A.J., 2002. A major perturbation of the carbon cycle before the ghaub glaciation (Neoproterozoic) in namibia: prelude to snowball earth? Geochem. Geophys. Geosyst. 3 (6), 1–24. https://doi.org/10.1029/2001GC000244.

Halverson, G.P., Hoffman, P.F., Schrag, D.P., Maloof, A.C., Rice, A.H.N., 2005. Toward a Neoproterozoic composite carbon-isotope record. Geol. Soc. Am. Bull. 117 (9–10), 1181–1207. https://doi.org/10.1130/B25630.1.

Halverson, G.P., Dudás, F., Maloof, A.C., Bowring, S.A., 2007. Evolution of the $^{87}Sr/^{86}Sr$ composition of neoproterozoic seawater. Palaeogeogr. Palaeoclimatol. Palaeoecol. 256 (3), 103–129. https://doi.org/10.1016/j.palaeo.2007.02.028.

Handley, L., Pearson, P.N., McMillan, I.K., Pancost, R.D., 2008. Large terrestrial and marine carbon and hydrogen isotope excursions in a new paleocene/eocene boundary section from Tanzania. Earth Planet. Sci. Lett. 275 (1–2), 17–25. https://doi.org/10.1016/j.epsl.2008.07.030.

Hermoso, M., Chan, I.Z.X., McClelland, H.L.O., Heureux, A.M.C., Rickaby, R.E.M., 2016. Vanishing coccolith vital effects with alleviated carbon limitation. Biogeosciences 13, 301–312. https://doi.org/10.5194/bgd-12-15835-2015.

Higgins, J.A., Blättler, C.L., Lundstrom, E.A., Santiago-Ramos, D.P., Akhtar, A.A., Crüger Ahm, A.S., et al., 2018. Mineralogy, early marine diagenesis, and the chemistry of shallow-water carbonate sediments. Geochim. Cosmochim. Acta 220, 512–534. https://doi.org/10.1016/j.gca.2017.09.046.

Hottinger, L., 1997. Shallow benthic foraminiferal assemblages as signals for depth of their deposition and their limitations. Bull. Soc. Géol. Fr. 168 (4), 491–505.

Hottinger, L., 1998. Shallow benthic foraminifera at the paleocene-eocene boundary. Strata 9 (1), 61–64.

Hottinger, L., 2006. The depth-depending ornamentation of some lamellar-perforate foraminifera. Symbiosis *42*, 141–154.

Husson, J.M., Higgins, J.A., Maloof, A.C., Schoene, B., 2015. Ca and Mg isotope constraints on the origin of Earth's deepest $\delta^{13}C$ excursion. Geochim. Cosmochim. Acta 160, 243–266. https://doi.org/10.1016/j.gca.2015.03.012.

Iglesias-Rodriguez, M.D., Halloran, P.R., Rickaby, R.E.M., Hall, I.R., Colmenero-Hidalgo, E., Gittins, J.R., et al., 2008. Phytoplankton calcification in a high-CO_2 world. Science 320 (5874), 336–340. https://doi.org/10.1126/science.1154122.

Jacobsen, S.B., Kaufman, A.J., 1999. The Sr, C and O isotopic evolution of neoproterozoic seawater. Chem. Geol. 161 (1), 37–57. https://doi.org/10.1016/S0009-2541(99)00080-7.

Kaufman, A.J., Knoll, A.H., 1995. Neoproterozoic variations in the C-isotopic composition of seawater: stratigraphic and biogeochemical implications. Precambrian Res. 73 (1), 27–49. https://doi.org/10.1016/0301-9268(94)00070-8.

Kaufman, A.J., Hayes, J.M., Knoll, A.H., Germs, G.J.B., 1991. Isotopic compositions of carbonates and organic carbon from upper proterozoic successions in namibia: stratigraphic variation and the effects of diagenesis and metamorphism. Precambrian Res. 49 (3), 301–327. https://doi.org/10.1016/0301-9268(91)90039-D.

Kelly, D.C., Nielsen, T.M.J., Schellenberg, S.A., 2012. Carbonate saturation dynamics during the paleocene-eocene thermal maximum: bathyal constraints from ODP sites 689 and 690 in the Weddell Sea (South Atlantic). Mar. Geol. 303–306, 75–86. https://doi.org/10.1016/j.margeo.2012.02.003.

Kennett, J.P., Stott, L.D., 1991. Abrupt deep-sea warming, palaeoceanographic changes and benthic extinctions at the end of the palaeocene. Nature 353 (6341), 225–229. https://doi.org/10.1038/353225a0.
Keul, N., Langer, G., Thoms, S., de Nooijer, L.J., Reichart, G.-J., Bijma, J., 2017. Exploring foraminiferal Sr/Ca as a new carbonate system proxy. Geochim. Cosmochim. Acta 202, 374–386. https://doi.org/10.1016/j.gca.2016.11.022.
Knauth, L.P., Kennedy, M.J., 2009. The late precambrian greening of the earth. Nature 460, 728–732. https://doi.org/10.1038/nature08213.
Koch, P.L., Zachos, J.C., Gingerich, P.D., 1992. Correlation between isotope records in marine and continental carbon reservoirs near the palaeocene/eocene boundary. Nature 358 (6384), 319–322. https://doi.org/10.1038/358319a0.
Kozdon, R., Ushikubo, T., Kita, N.T., Spicuzza, M., Valley, J.W., 2009. Intratest oxygen isotope variability in the planktonic foraminifer *N. pachyderma*: real vs. apparent vital effects by ion microprobe. Chem. Geol. 258 (3–4), 327–337. https://doi.org/10.1016/j.chemgeo.2008.10.032.
Kozdon, R., Kelly, D.C., Kitajima, K., Strickland, A., Fournelle, J.H., Valley, J.W., 2013. In situ $\delta^{18}O$ and Mg/Ca analyses of diagenetic and planktic foraminiferal calcite preserved in a deep-sea record of the paleocene-eocene thermal maximum. Paleoceanography 28 (3), 517–528. https://doi.org/10.1002/palo.20048.
Kozdon, R., Kelly, D.C., Valley, J.W., 2018. Diagenetic attenuation of carbon isotope excursion recorded by planktic foraminifers during the paleocene-eocene thermal maximum. Paleoceanography Paleoclimatol. 33 (4), 367–380. https://doi.org/10.1002/2017PA003314.
Lea, D., 1999. Trace elements in foraminiferal calcite. In: Sen Gupta, B.K. (Ed.), Modern Foraminifera. Kluwer Academic Publishers, Dordrecht, pp. 259–277.
Lea, D.W., Mashiotta, T.A., Spero, H.J., 1999. Controls on magnesium and strontium uptake in planktonic foraminifera determined by live culturing. Geochim. Cosmochim. Acta 63 (16), 2369–2379. https://doi.org/10.1016/S0016-7037(99)00197-0.
Leppig, U., 1988. Structural analysis and taxonomic revision of *Miscellanea*, Paleocene, larger Foraminifera. Eclogae Geol. Helv. 81 (3), 689–721.
Li, J., Hu, X., Garzanti, E., BouDagher-Fadel, M., 2017. Shallow-water carbonate responses to the paleocene-eocene thermal maximum in the tethyan Himalaya (southern Tibet): tectonic and climatic implications. Palaeogeogr. Palaeoclimatol. Palaeoecol. 466, 153–165. https://doi.org/10.1016/j.palaeo.2016.11.026.
Magioncalda, R., Dupuis, C., Smith, T., Steurbaut, E., Gingerich, P.D., 2004. Paleocene-Eocene carbon isotope excursion in organic carbon and pedogenic carbonate: direct comparison in a continental stratigraphic section. Geology 32 (7), 553–556. https://doi.org/10.1130/G20476.1.
Manners, H.R., Grimes, S.T., Sutton, P.A., Domingo, L., Leng, M.J., Twitchett, R.J., et al., 2013. Magnitude and profile of organic carbon isotope records from the paleocene-eocene thermal maximum: evidence from northern Spain. Earth Planet. Sci. Lett. 376, 220–230. https://doi.org/10.1016/j.epsl.2013.06.016.
Marshall, J.D., 1992. Climatic and oceanographic isotopic signals from the carbonate rock record and their preservation. Geol. Mag. 129 (2), 143–160.
McCarren, H., Thomas, E., Hasegawa, T., Röhl, U., Zachos, J.C., 2008. Depth dependency of the paleocene-eocene carbon isotope excursion: paired benthic and terrestrial biomarker records (ocean drilling program Leg 208, Walvis Ridge). Geochem. Geophys. Geosyst. 9 (10), Q10008. https://doi.org/10.1029/2008GC002116.
McInerney, F.A., Wing, S.L., 2011. The paleocene-eocene thermal maximum: a perturbation of carbon cycle, climate, and biosphere with implications for the future. Annu. Rev. Earth Planet. Sci. 39 (1), 489–516. https://doi.org/10.1146/annurev-earth-040610-133431.
Meissner, K.J., Bralower, T.J., Alexander, K., Jones, T.D., Sijp, W., Ward, M., 2014. The paleocene-eocene thermal maximum: how much carbon is enough? Paleoceanography 29 (10), 946–963. https://doi.org/10.1002/2014PA002650.
Munnecke, A., Westphal, H., Reijmer, J.J.G., Samtleben, C., 1997. Microspar development during early marine burial diagenesis: a comparison of pliocene carbonates from the Bahamas with silurian limestones from Gotland (Sweden). Sedimentology 44 (6), 977–990. https://doi.org/10.1111/j.1365-3091.1997.tb02173.x.
Nabelek, P.I., 1987. General equations for modeling fluid/rock interaction using trace elements and isotopes. Geochim. Cosmochim. Acta 51 (6), 1765–1769. https://doi.org/10.1016/0016-7037(87)90354-1.
Nicolo, M.J., Dickens, G.R., Hollis, C.J., 2010. South Pacific intermediate water oxygen depletion at the onset of the Paleocene-Eocene thermal maximum as depicted in New Zealand margin sections. Paleoceanography 25 (4), PA4210. https://doi.org/10.1029/2009PA001904.
Nunes, F., Norris, R.D., 2006. Abrupt reversal in ocean overturning during the Palaeocene/Eocene warm period. Nature 439 (7072), 60–63. https://doi.org/10.1038/nature04386.
Pagani, M., Pedentchouk, N., Huber, M., Sluijs, A., Schouten, S., Brinkhuis, H., et al., 2006. Arctic hydrology during global warming at the palaeocene/eocene thermal maximum. Nature 442 (7103), 671–675. https://doi.org/10.1038/nature05043.
Panchuk, K., Ridgwell, A., Kump, L.R., 2008. Sedimentary response to paleocene-eocene thermal maximum carbon release: a model-data comparison. Geology 36 (4), 315–318. https://doi.org/10.1130/G24474A.1.
Papazzoni, C.A., Cosovic, V., Briguglio, A., Drobne, K., 2017. Towards a calibrated larger foraminifera biostratigraphic zonation: celebrating 18 years of the application of shallow benthic zones. Palaios 32 (1), 1–5. https://doi.org/10.2110/palo.2016.043.
Pearson, P.N., Ditchfield, P.W., Singano, J., Harcourt-Brown, K.G., Nicholas, C.J., Olsson, R.K., et al., 2001. Warm tropical sea surface temperatures in the late cretaceous and eocene epochs. Nature 413, 481–487. https://doi.org/10.1038/35097000.
Röhl, U., Westerhold, T., Bralower, T.J., Zachos, J.C., 2007. On the duration of the paleocene-eocene thermal maximum (PETM). Geochem. Geophys. Geosyst. 8 (12), Q12002. https://doi.org/10.1029/2007GC001784.
Rohling, E.J., Sluijs, A., Dijkstra, H.A., Köhler, P., Wal, R.S.W., Heydt, A.S., et al., 2012. Making sense of palaeoclimate sensitivity. Nature 491 (7426), 683–691. https://doi.org/10.1038/nature11574.
Sadler, P.M., 1981. Sediment accumulation rates and the completeness of stratigraphic sections. J. Geol. 89 (5), 569–584. https://doi.org/10.1086/628623.
Sadler, P.M., 1999. The influence of hiatuses on sediment accumulation rates. Geores. Forum 5, 15–40.
Schmidt, C., Heinz, P., Kucera, M., Uthicke, S., 2011. Temperature-induced stress leads to bleaching in larger benthic foraminifera hosting endosymbiotic diatoms. Limnol. Oceanogr. 56 (5), 1587–1602. https://doi.org/10.4319/lo.2011.56.5.1587.
Schmidt, C., Kucera, M., Uthicke, S., 2014. Combined effects of warming and ocean acidification on coral reef Foraminifera *Marginopora vertebralis* and *Heterostegina depressa*. Coral Reefs 33 (3), 805–818. https://doi.org/10.1007/s00338-014-1151-4.
Schmitz, B., Pujalte, V., 2003. Sea-level, humidity, and land-erosion records across the initial eocene thermal maximum from a continental-marine transect in northern Spain. Geology 31 (8), 689–692. https://doi.org/10.1130/G19527.1.
Schubert, B.A., Jahren, A.H., 2013. Reconciliation of marine and terrestrial carbon isotope excursions based on changing atmospheric CO_2 levels. Nat. Commun. 4, 1653. https://doi.org/10.1038/ncomms2659.
Schumer, R., Jerolmack, D.J.C.F.A., 2009. Real and apparent changes in sediment deposition rates through time. J. Geophys. Res. 114 (F3), F00A06. https://doi.org/10.1029/2009JF001266.
Serra-Kiel, J., Hottinger, L., Caus, E., Drobne, K., Ferrandez, C., Jauhri, A.K., et al., 1998. Larger foraminiferal biostratigraphy of the tethyan paleocene and eocene. Bull. Soc. Geol. Fr. 169 (2), 281–299.
Sexton, P.F., Wilson, P.A., Pearson, P.N., 2006. Microstructural and geochemical perspectives on planktic foraminiferal preservation: “Glassy” versus “Frosty”. Geochem. Geophys. Geosyst. 7 (12). https://doi.org/10.1029/2006GC001291.
Siahi, M., Hofmann, A., Master, S., Wilson, A., Mayr, C., 2018. Trace element and stable (C, O) and radiogenic (Sr) isotope geochemistry of stromatolitic carbonate rocks of the mesoarchaean pongola supergroup: implications for seawater composition. Chem. Geol. 476, 389–406. https://doi.org/10.1016/j.chemgeo.2017.11.036.
Sluijs, A., Brinkhuis, H., Crouch, E.M., John, C.M., Handley, L., Munsterman, D., et al., 2008. Eustatic variations during the paleocene-eocene greenhouse world. Paleoceanography 23. https://doi.org/10.1029/2008PA001615.
Smith, F.A., Wing, S.L., Freeman, K.H., 2007. Magnitude of the carbon isotope excursion at the paleocene-eocene thermal maximum: the role of plant community change. Earth Planet. Sci. Lett. 262 (1–2), 50–65. https://doi.org/10.1016/j.epsl.2007.07.021.
Spero, H.J., Lerche, I., Williams, D.F., 1991. Opening the carbon isotope “vital effect” black box, 2, Quantitative model for interpreting foraminiferal carbon isotope data. Paleoceanography 6 (6), 639–655. https://doi.org/10.1029/91PA02022.
Stoll, H.M., 2005. Limited range of interspecific vital effects in coccolith stable isotopic records during the paleocene-eocene thermal maximum. Paleoceanography 20 (1), PA1007. https://doi.org/10.1029/2004PA001046.
Swart, P.K., Eberli, G., 2005. The nature of the $\delta^{13}C$ of periplatform sediments: implications for stratigraphy and the global carbon cycle. Sediment. Geol. 175, 115–129. https://doi.org/10.1016/j.sedgeo.2004.12.029.
Swart, P.K., Kennedy, M.J., 2012. Does the global stratigraphic reproducibility of $\delta^{13}C$ in neoproterozoic carbonates require a marine origin? a pliocene–pleistocene comparison. Geology 40 (1), 87–90. https://doi.org/10.1130/G32538.1.
Talge, H.K., Hallock, P., 2003. Ultrastructural responses in field-bleached and experimentally stressed *Amphistegina gibbosa* (Class Foraminifera). J. Eukaryot. Microbiol. 50 (5), 324–333. https://doi.org/10.1111/j.1550-7408.2003.tb00143.x.
Thomas, E., Shackleton, N.J., 1996. The paleocene-eocene benthic foraminiferal extinction and stable isotope anomalies. In: Knox, R.W.O.B., Corfield, R.M., Dunay, R.E. (Eds.), Correlation of the Early Paleogene in Northwest Europe. Geological Society London Special Publications, London, pp. 401–441.
Thomas, D.J., Zachos, J.C., Bralower, T.J., Thomas, E., Bohaty, S., 2002. Warming the fuel for the fire: evidence for the thermal dissociation of methane hydrate during the paleocene-eocene thermal maximum. Geology 30 (12), 1067–1070. https://doi.org/10.1130/0091-7613(2002)030<1067:WTFFTF>2.0.CO;2.
Tipple, B.J., Pagani, M., Krishnan, S., Dirghangi, S.S., Galeotti, S., Agnini, C., et al., 2011. Coupled high-resolution marine and terrestrial records of carbon and hydrologic cycles variations during the Paleocene-Eocene Thermal Maximum (PETM). Earth Planet. Sci. Lett. 311 (1–2), 82–92. https://doi.org/10.1016/j.epsl.2011.08.045.
Valley, J.W., Kita, N.T., 2009. *In situ* oxygen isotope geochemistry by ion microprobe. In: Fayek, M. (Ed.), Secondary Ion Mass Spectrometry in the Earth Sciences. 41. Mineralogical association of Canada short course, Toronto, pp. 19–63.
van Hinsbergen, D.J.J., Lippert, P.C., Dupont-Nivet, G., McQuarrie, N., Doubrovine, P.V., Spakman, W., Torsvik, T.H., 2012. Greater India basin hypothesis and a two-stage cenozoic collision between India and Asia. Proc. Natl. Acad. Sci. 109 (20), 7659–7664. https://doi.org/10.1073/pnas.1117262109.
Yans, J., Strait, S.G., Smith, T., Dupuis, C., Steurbaut, E., Gingerich, P.D., 2006. High-resolution carbon isotope stratigraphy and mammalian faunal change at the paleocene-eocene boundary in the honeycombs area of the southern Bighorn Basin, Wyoming. Am. J. Sci. 306 (9), 712–735. https://doi.org/10.2475/09.2006.02.
Yu, J., Elderfield, H., Jin, Z., Tomascak, P., Rohling, E.J., 2014. Controls on Sr/Ca in benthic foraminifera and implications for seawater Sr/Ca during the late Pleistocene. Quat. Sci. Rev. 98, 1–6. https://doi.org/10.1016/j.quascirev.2014.05.018.
Zachos, J.C., Wara, M.W., Bohaty, S., Delaney, M.L., Petrizzo, M.R., Brill, A., et al., 2003. A transient rise in tropical sea surface temperature during the paleocene-eocene thermal maximum. Science 302 (5650), 1551–1554. https://doi.org/10.1126/science.1090110.
Zachos, J.C., Rohl, U., Schellenberg, S.A., Sluijs, A., Hodell, D.A., Kelly, D.C., et al., 2005. Rapid acidification of the ocean during the paleocene-eocene thermal maximum. Science 308 (5728), 1611–1615. https://doi.org/10.1126/science.1109004.

Zachos, J.C., Bohaty, S.M., John, C.M., McCarren, H., Kelly, D.C., Nielsen, T., 2007. The palaeocene–eocene carbon isotope excursion: constraints from individual shell planktonic foraminifer records. Phil. Trans. R. Soc. A 365 (1856), 1829–1842. https://doi.org/10.1098/rsta.2007.2045.

Zachos, J.C., Dickens, G.R., Zeebe, R.E., 2008. An early Cenozoic perspective on greenhouse warming and carbon-cycle dynamics. Nature 451 (7176), 279–283. https://doi.org/10.1038/nature06588.

Zamagni, J., Mutti, M., Ballato, P., KoÅir, A., 2012. The Paleocene-Eocene thermal maximum (PETM) in shallow-marine successions of the Adriatic carbonate platform (SW Slovenia). Geol. Soc. Am. Bull. 124 (7–8), 1071–1086. https://doi.org/10.1130/b30553.1.

Zeebe, R.E., Zachos, J.C., Dickens, G.R., 2009. Carbon dioxide forcing alone insufficient to explain palaeocene-eocene thermal maximum warming. Nat. Geosci. 2 (8), 576–580. https://doi.org/10.1038/ngeo578.

Zhang, Q., Wendler, I., Xu, X., Willems, H., Ding, L., 2017. Structure and magnitude of the carbon isotope excursion during the paleocene-eocene thermal maximum. Gondwana Res. 46, 114–123. https://doi.org/10.1016/j.gr.2017.02.016.

Zhang, Q., Willems, H., Ding, L., Xu, X., 2019. Response of larger benthic foraminifera to the paleocene-eocene thermal maximum and the position of the paleocene/eocene boundary in the tethyan shallow benthic zones: evidence from South Tibet. Geol. Soc. Am. Bull. 131, 84–98. https://doi.org/10.1130/B31813.1.

Zhu, M., Ding, Z., Wang, X., Chen, Z., Jiang, H., Dong, X., et al., 2010. High-resolution carbon isotope record for the paleocene-eocene thermal maximum from the Nanyang Basin, Central China. Chin. Sci. Bull. 55 (31), 3606–3611. https://doi.org/10.1007/s11434-010-4092-5.